NIH Public Access
Author Manuscript
*Nanotechnology*. Author manuscript; available in PMC 2012 December 9.

Published in final edited form as:
*Nanotechnology*. 2011 December 9; 22(49): 494015. doi:10.1088/0957-4484/22/49/494015.

# Tailoring material properties of a nanofibrous extracellular matrix derived hydrogel

**Todd D. Johnson**, **Stephen Y. Lin**, and **Karen L. Christman***
Department of Bioengineering University of California, San Diego 9500 Gilman Drive MC 0412 La Jolla, CA 92093-0412

## Abstract

In the native tissue, the interaction between cells and the extracellular matrix (ECM) is essential for cell migration, proliferation, differentiation, mechanical stability, and signaling. It has been shown that decellularized ECMs can be processed into injectable formulations, thereby allowing for minimally invasive delivery. Upon injection and increase in temperature, these materials self-assemble into porous gels forming a complex network of fibers with nano-scale structure. In this study we aimed to examine and tailor the material properties of a self-assembling ECM hydrogel derived from porcine myocardial tissue, which was developed as a tissue specific injectable scaffold for cardiac tissue engineering. The impact of gelation parameters on ECM hydrogels has not previously been explored. We examined how modulating pH, temperature, ionic strength, and concentration affected the nanoscale architecture, mechanical properties, and gelation kinetics. These material characteristics were assessed using scanning electron microscopy, rheometry, and spectrophotometry, respectively. Since the main component of the myocardial matrix is collagen, many similarities between the ECM hydrogel and collagen gels were observed in terms of the nanofibrous structure and modulation of properties by altering ionic strength. However, variation from collagen gels was noted for the gelation temperature along with varied times and rates of gelation. These discrepancies when compared to collagen are likely due to the presence of other ECM components in the decellularized ECM based hydrogel. These results demonstrate how the material properties of ECM hydrogels could be tailored for future *in vitro* and *in vivo* applications.

### Keywords

decellularization; extracellular matrix; injectable; hydrogel; biomaterial

## 1. Introduction

The extracellular matrix (ECM) is a complex mixture of proteins, proteoglycans (PGs) and glycosaminoglycans (GAGs) [1-4], which provides cells with a dynamic three-dimensional environment inherent with a nanoscale architecture [5]. ECM components, such as fibrous collagen, have nanoscale structures that are important for cell-matrix interactions via membrane bound integrin proteins [5-7]. These interactions are essential for cell migration, proliferation, differentiation, mechanical stability, and signaling [6, 8-10]. The field of tissue engineering aims to create and tailor the extracellular environment by creating custom scaffolds for both *in vivo* and *in vitro* studies and applications [11-14]. One method of scaffold design is to utilize or mimic the native environment, including tissue specific biochemical composition and structure [15-17]. Mimicking the inherent cell-matrix interactions by creating the appropriate biological and chemical cues can tailor the

* christman@bioeng.ucsd.edu .

NIH-PA Author Manuscript
NIH-PA Author Manuscript
NIH-PA Author Manuscript

NIH-PA Author Manuscript

NIH-PA Author Manuscript

NIH-PA Author Manuscript

differentiation, proliferation, migration of cells *in vitro* and tissue regeneration *in vivo* [6, 13].

The most characterized and prominent component of the ECM is collagen. Collagen is a fibrous protein that is used for numerous applications in science and medicine including tissue culture coatings, burn-victim dressings, drug delivery, and cosmetic injections [14, 18]. Native collagen can be processed into an injectable solubilized form, which can self-assemble under certain conditions into a hydrogel with nanoscale fibrous structure [8, 19, 20]. The material properties and cell-matrix interactions of these gels have been well characterized. For example, varying temperature, ion concentration, phosphate content, pH, and material concentration is known to alter gelation kinetics, stiffness, and the nanoscale fibrous architecture of the collagen hydrogels [19-24].

Collagen is, however, a single component of the ECM and cannot fully mimic the biochemical complexity of the cells native environment. This limitation has motivated the development of more complex materials including Matrigel, decellularized tissues [17], and mixtures of single proteins (ie. collagen, fibronectin, elastin) with other ECM components (ie. PGs, GAGs) [8, 11, 13, 25, 26]. Decellularized tissues can be further processed into liquids and used to create gels with porous fibrous nanostructures similar to the collagen hydrogels [27-29]. Each tissue in the body contains a unique ECM, so decellularized materials have distinctive compositions specific to their tissue of origin [25, 29]. This diversity allows for the development of tissue-specific scaffolds for appropriate cell-matrix interactions. So far, ECM hydrogels derived from small intestinal submucosa (SIS), adipose tissue, bladder, pericardium and myocardium have been reported [29-33]. The effect of cross-linking on hydrogel stiffness, degradation properties, and cell migration has been examined with an ECM hydrogel [34]; however, no studies have examined how gelation kinetics, stiffness, swelling ratio, and nanoscale architecture of ECM derived hydrogels can be modulated through altering gelation conditions. Unlike collagen, the modulation of ECM matrix gelation parameters in order to tailor the material properties has not been explored. In this study we aimed to tailor the material properties of a self-assembling ECM hydrogel and investigate the effect of varying temperature, ionic strength, pH, and material concentration on material properties. The ECM material was analyzed with scanning electron microscopy (SEM) to characterize the nano-scale architecture, rheometry to measure stiffness and viscosity, and spectrophotometry to assess gelation kinetics. An ECM hydrogel derived from porcine myocardial tissue was selected for analysis in this study. This myocardial matrix material was developed as a tissue specific injectable scaffold for cardiac tissue engineering [29]. Several injectable materials, including synthetic and naturally derived materials such as the myocardial ECM hydrogel invested here, have shown promise for treating myocardial infarction, and this field has rapidly expanded in recent years [35-38].

## 2. Methods and Materials

### 2.1 Tissue Decellularization and Material Processing

Porcine myocardial tissue was harvested and decellularized following a modified version of a previously reported protocol [29]. In brief, the left ventricle was sliced into small pieces and decellularized in a solution of 1% (wt/vol) sodium dodecyl sulfate (SDS) (Fischer Scientific, Hanover Park, IL), phosphate buffered saline (PBS), and 0.5% Penicillin/ Streptomycin (GIBCO, Invitrogen, Carlsbad, CA). Once decellularized after 3-5 days with daily solution changes, the tissue was rinsed with water to remove residual SDS then frozen at -80°C. The frozen decellularized material was lyophilized, and milled into a fine powder using a Wiley Mini Mill. The powder was stored at -80°C until needed for use.

NIH-PA Author Manuscript

NIH-PA Author Manuscript

NIH-PA Author Manuscript

### 2.2 ECM Gel Formation

The extracellular matrix material was enzymatically digested by adding a 1 mg/ml solution of pepsin (Sigma, St. Louis, MO) in 0.1 M HCl such that the final concentration of material was 10 mg/ml [29]. The material was digested for 48-60 hours at room temperature with constant stirring until the liquid was homogeneous with no visible particles. The pH (7.4 or 8.5) and salt concentration (0.5×, 1.0×, or 1.5× PBS) was adjusted using 1.0 M NaOH and 10× PBS, respectively, to end with the desired final material concentration (6 mg/ml or 8 mg/ml). The final mixture was then allowed to gel for 24 hours at 4°C, 22°C, or 37°C. Standard conditions are defined as physiological conditions of pH 7.4, 1.0x PBS, and 37°C. Only one parameter (temperature, salt concentration or pH) at a time was varied away from these standard conditions for any of the following experiments.

### 2.3 Scanning Electron Microscopy

The gels were crosslinked with 2.5% glutaraldehyde (Sigma-Aldrich, Grade II, 25%, St. Louis, MO) for 2 hours then dehydrated with a series of ethanol washes of increasing concentration (30%, 50%, 75%, and 100%). After storing overnight in 100% ethanol, the gels were critical point dried from ethanol in $CO_2$ using a Tousimis AutoSamdri 815A. Samples were mounted and then sputter coated with Chromium (Cr) or Iridium (Ir) using an Emitech K575X Sputter Coater [39]. Imaging was done with a FEI XL30 UHR SEM. All conditions were done in triplicate and images were taken at 5,000× and 20,000×. Three images taken at random locations at 20,000× were used to measure fiber diameter for each sample. The widths of at least 10 distinguishable fibers per image were measured using AxioVision software. An unbiased method was applied to select the fibers to be measured, which involved drawing a series of diagonal lines across the image [40].

### 2.4 Rheometry: Storage Modulus, Loss Modulus, and Viscosity

Rheological and viscometric measurements were made with a TA Instruments ARG2 Rheometer. Modified from a previous method, a parallel-plate geometry (20mm diameter) at 1.2mm gap height was used on 500 uL gels of the different conditions after 24 hours of gelation [41]. For each condition, the storage modulus (G') and loss modulus (G”) over frequencies of 0.04-16 Hz were recorded for every gel condition in triplicate. The storage modulus at 1 rad/s or 0.16 Hz was plotted for each condition.

For viscometric measurements, samples were prepared as discussed earlier and kept on ice until experimentation. The rheometer was preheated and maintained at 25°C. Then 200 uL of sample was loaded into the rheometer set at 500 μm gap height such that sample completely filled the gap. Measurements of viscosity were made over a frequency range of 0.1 - 50 Hz as previously reported [42]. The data was best-fit to the following power law:

$$\eta = k f^n \tag{1}$$

In this equation ($\eta$) is the complex viscosity and ($f$) is frequency, with ($k$) and ($n$) being constants.

### 2.5 Swelling Ratio

ECM gels of 250 uL for each condition in triplicate were formed in a 48-well plate for 24 hours at 37°C. The gels were transferred to a 12-well plate and were allowed to swell in PBS for 24 hours. The samples were removed, carefully blotted to remove excess surface liquid, and the total swelled weight was measured ($W_s$). Then the samples were fully dried using a vacuum desiccator overnight and total dry weight was measured ($W_d$). Swelling ratios were calculated as:

NIH-PA Author Manuscript

NIH-PA Author Manuscript

NIH-PA Author Manuscript

$$Swelling \quad Ratio = \frac{W_s - W_d}{W_d} \tag{2}$$

### 2.6 Turbidimetric gelation kinetics

Turbidimetric gelation kinetics were determined through spectrophotometric measurements as previously described [43]. First, a Synergy® 4 Multi-Mode Microplate Reader (Biotek) was preheated to 37°C. Then 100 uL of each ECM sample, prepared as previously described, was placed into a 96 well plate in triplicate. Absorbance was measured at 405 nm wavelength every minute for 8 hours or until the data plateaued. Absorbance values were averaged within each group, normalized, and plotted over time. From the normalized plot, a linear fit was applied to the linear region of the plot to calculate the half time of gelation ($t_{1/2}$), the lag phase ($t_{lag}$), and the slope or speed of gelation ($S$). Half time of gelation was defined as the time when the material reached 50% of the maximum measured absorbance. The lag phase was calculated by finding the time at which the linear-fit was zero for normalized absorbance.

### 2.7 Statistical Analysis

All values were reported as mean ± standard deviation. Samples were run in triplicate and significance accepted at $p < 0.05$. Significance of the data was assessed using either an unpaired student's t-test or a one-way ANOVA with a Tukey or Dunnett's post-test. Complex viscosity in triplicate were averaged and then fit to the power law (1). Significance for complex viscosity was determined by comparing the two concentrations at 10 Hz.

## 3. Results

### 3.1 Effect of Temperature

The gelation temperature is an important parameter for self-assembling hydrogels when considering them as injectable materials for clinical applications, particularly their ability to gel at body temperature. Once processed, the myocardial matrix material is a free flowing liquid and upon increasing the temperature it forms into a gel (figure 1). The material at physiological pH and salt concentrations, when stored at either 4°C or room temperature for 24 hours, remained a liquid. Increasing the concentration from 6 to 8 mg/mL did not result in gelation at these temperatures. However, when incubated at 37°C, the material self-assembled into a gel that maintained shape at both concentrations (figure 1).

Scanning electron microscopy (SEM) was used to assess the presence of a nanoscale fibrous structure at each of the temperatures for both concentrations at standard physiological conditions. The images were used to verify which temperatures produced fibril formations. The SEM images at 20,000× confirmed that the material did not form a nanoscale fibrous network at the two lower temperatures for either concentration whereas at 37°C, fibers were formed (figure 2). The lower two temperatures tested had some singular fibers, but the majority of the material was solid and nonporous as a result of the glutaraldehyde crosslinking during processing for SEM. Both material concentrations at 37°C had clear interwoven networks of linear fibers indicating successful fibrillogenesis. The morphologies for both concentrations at 37°C were similar but showed great variation from location to location when viewed at 20,000×. This fluctuation in local density and morphology is better shown in the 5,000x images in figure 3. Since 4°C and 22°C did not form gels at 6 mg/ml and 8 mg/ml, these groups were not examined in subsequent experiments.

NIH-PA Author Manuscript

NIH-PA Author Manuscript

NIH-PA Author Manuscript

### 3.2 Effect of ionic strength, pH, and concentration

**3.2.1 Scanning Electron Microscopy—**The gels under each of the explored conditions were imaged using SEM to confirm fiber formation and analyze the fibrous structure. Gelation and the formation of a nanofibrous structure occurred for the test ranges of salt concentration (0.5× - 1.5× PBS), pH level (7.4 - 8.5), and concentrations of the myocardial matrix material (6 - 8 mg/ml) as confirmed by SEM images at 5,000× in figure 3. A complex network of nanoscale fibers was consistently formed for each condition. However, each of the gels displayed inhomogeneity of the fiber matrix density; regions of increased and decreased fiber density within a single gel made it difficult to assess the overall fiber matrix from the SEM images. These variations in densities at the nanoscale can be observed in figure 3.

Images were also taken at 20,000× and used to analyze the impact of salt, pH, and material concentration on fiber diameter (figure 4). No statistically significant changes in average fiber diameter were observed when varying each of these parameters (table 1). Average fiber diameter was consistently around 100nm for all conditions with distributions over the range of 30nm to 250nm.

**3.2.2 Rheometry: Storage Modulus, Loss Modulus, and Viscosity—**Rheometry was used to measure the storage modulus and loss modulus of the gels at each condition to determine if salt, pH, or material concentration alters the mechanical properties of the gels (table 2). The storage modulus for the four conditions at 6 mg/ml ranged from 2.58-10.23 Pa and the 8 mg/ml gels were 5.94-12.36 Pa. Increasing material concentration from 6 mg/ml to 8 mg/ml consistently produced gels with a trend of higher storage modulus for all conditions, thus increasing concentration leads to stiffer gels. Raising salt concentration lead to a significant decrease in the storage modulus (G') of the 6 mg/ml gels with a similar trend observed for the 8 mg/ml group as shown in figure 5a. When salt concentration was increased from 1.5× PBS to 0.5× PBS the storage modulus more than tripled on average at 6 mg/ml and doubled at 8 mg/ml. The changes in material properties of the gels with alterations in salt concentration were also observed during their handling. This indicates that the concentration of salt ions in solutions impacts the fibrillogenesis of the myocardial matrix leading to changes in the bulk material properties of the hydrogels. When increasing the pH from 7.4 to 8.5 no significant change in the storage modulus was measured for either material concentration (figure 5b). A ten-fold modulation in proton concentration had less of an impact on the storage modulus than decreasing the salt concentration by half. Increased gel stiffness was still observed with increasing material concentration, with significance at both pH 7.4 and pH 8.5. The loss modulus (G”) followed the same trends as the storage modulus (table 2). The loss modulus for each of the conditions had a range of 0.467-1.652 Pa and 1.70-2.72 Pa for the 6 and 8 mg/ml samples, respectively. Once again, there was more than a three-fold increase in the loss modulus as the salt concentration decreased from 1.5× PBS to 0.5× PBS for the 6 mg/ml samples and almost doubled for the 8 mg/ml samples. Also, as material concentration was increased there was a consistent trend of increasing loss modulus.

When considering a material for delivery via injection, the viscosity in the liquid state is important. The myocardial material was thus assessed over a range of shear rates and complex viscosity was measured using a rheometer. Complex viscosity for all samples decreased as shear rate increased, providing a linear trend when plotted on a log-log scale. Because of the linear nature of the data on a log-log scale, a power equation (1) was used to fit the data (table 3). The reported values of ($k$) and ($n$) are constants from the power equation used to fit the data. The coefficient of determination ($r^2$) indicates the accuracy of the power equation fit with a value of 1 indicating a perfect fit. Changes in complex

NIH-PA Author Manuscript

NIH-PA Author Manuscript

NIH-PA Author Manuscript

viscosity between the different conditions were only observed for different material concentrations with pH and salt concentration having no effect. Increasing the myocardial ECM concentration when in liquid form creates increased intermolecular forces leading to an increase in viscosity. There was a significant increase in complex viscosity when material concentration was increased at standard conditions ($p = 0.0001$) and this can be observed as vertical shift of the data points in figure 6. This trend is also confirmed by the increase in the (*k)* values between the 6 mg/ml and 8 mg/ml samples (table 3). Since plotted on a log-log scale, the negative values for (*n*) correlate to the slope and indicate that the material is shear thinning. The (n) values for the 6 mg/ml range from -0.466 to -0.550 and are significantly larger than the 8 mg/ml values, which range from -0.580 to -0.656, and this slight variation in slope can be observed in figure 6. Because the material is shear thinning, it will have a lower viscosity when experiencing higher shear rates, such as those that occur when passing through a catheter or needle during an injection.

### 3.3 Swelling Ratio

Swelling ratios by mass for the five conditions at both material concentrations are summarized in table 4. The mean values for swelling ratio ranged from 55.7 - 58.4 and did not show any significant variation between the groups.

### 3.4 Turbidimetric gelation kinetics

We observed marked changes in gelation when varying salt concentration, and therefore next performed turbidimetric assessment to quantify gelation kinetics. The absorbance of the gels at 405 nm was measured to analyze the turbidimetric gelation kinetics. The results for the material at 6 mg/ml, as absorbance and normalized absorbance plotted over time, are shown in figure 7. The calculated parameters $t_{1/2}$, $t_{lag}$, and $S$ from the linear fits are summarized in table 5. The results for 1.5× PBS were omitted because of the long gelation time. After 8 hours, the 1.5× PBS samples did not show an increase in absorbance and when visually inspected had not formed gels. When these gels were further incubated at 37°C for a total of 16 hours, gels were formed. Therefore, gelation time for 1.5× PBS samples ranges from 8 to 24 hours. Changing salt concentration had a significant effect on gelation kinetics. Samples with salt concentrations of 0.5× PBS had a significant decrease of $t_{1/2}$ and increase of slope (table 5). This indicates that lowering salt concentration shortens the gelation time with an increase in the rate of gelation. Thus, the observations of dramatically slower gelation at 1.5× PBS were consistent with these findings.

## 4. Discussion

Naturally derived ECM hydrogels have become a new biomaterial of investigation for use as a porous fibrous scaffold that is tissue specific [15, 28-30, 32]. These hydrogels produced from decellularized tissue can be processed into an injectable liquid material that gels via self-assembly at physiological conditions for pH, temperature, and salt concentration. While the native 3D structure is lost, ECM hydrogels are advantageous over intact decellularized tissues in that they can be delivered minimally invasively through a simple injection. Once gelled, the ECM hydrogels form a complex nanoscale mesh of fibers. This architecture is significant since in the native tissue there are nanoscale cell-matrix interactions via integrins that are important for cellular migration, proliferation, and differentiation [5, 6, 10]. Similar to other nanofibrous materials, ECM hydrogels have a high surface area-to-volume ratio providing increased area for integrin binding [12, 40]. Mauck et al. has emphasized the importance of characterizing tissue engineering constructs from their nanoscale fibrous formations to their macro-level material properties [44]. Scaffolds that provide a nanostructure and biochemical cues designed for tissue engineering and regenerative

NIH-PA Author Manuscript

NIH-PA Author Manuscript

NIH-PA Author Manuscript

medicine must be tailored to have the appropriated characteristics and material properties for a given application [6, 12-15].

In this study an ECM hydrogel developed from porcine myocardial tissue was more fully characterized to increase the understanding of modulating its material properties. Particular interest was placed on the parameters of gelation including temperature, salt concentration, pH, and material concentration since each has been shown to alter properties of collagen hydrogels. These parameters impacted the final material, which was assessed for gelation kinetics, viscosity, fibrous nanostructure, swelling ratio by mass, and stiffness. Soluble collagen is known to form gels at physiological pH and salt concentrations from 4°C to 37°C [19, 20]. However, the myocardial matrix showed a lack of gelation and fiber formation at lower temperatures (4°C and 22°C), indicating a difference in its response to temperature when compared to collagen. This is a beneficial attribute when considering this material for injection via catheter since it can maintain its liquid form at room temperature and gels once in the body at 37°C [15].

Each condition explored produced nanoscale fibrous structures with porous architectures when gelled at 37°C as shown in figure 5. Heterogeneity between different locations in the gels made it difficult to assess the overall tightness of the fiber matrix of each gel. This point-to-point variation in the composition of the myocardial matrix is consistent with results for collagen. Latinovic et al. showed a dramatic change of mechanical properties from location to location in self-assembled collagen gels indicating structural inhomogeneity [45]. It was hypothesized that this variation is due to the mechanism of self-assembly and the importance of nucleation sites for the formation of the fibrous structure [8, 45]. Thus, based off the local SEM images from this study, the overall organization and tightness of the material at the different conditions could not be determined. Analysis of the mean fiber diameter from the SEM images showed a consistent average fiber diameter of around 100nm with the range from below 30nm to over 250nm. The changes of the explored parameters did not lead to a significant shift of fiber diameter distributions. Collagen gels have showed varied fiber diameters depending on the conditions of gelation and have reported values similar to the myocardial matrix hydrogels [8, 19, 22, 23, 46-48].

Changes in salt concentration had the most dramatic impacts on stiffness and gelation kinetics. As salt concentration was increased, the rate of gelation decreased and half time of gelation significantly increased. For the 6 mg/ml gels at standard conditions, the material had a $t_{1/2}$, as determined by spectrophotometry, of 67.14 ± 3.40 minutes after incubation at 37°C. But, when concentration was increased to 1.5× PBS gelation took longer than 8 hours. Decreasing the salt concentration to 0.5× PBS rapidly decreased the $t_{1/2}$ down to 21.27 ± 2.33 minutes. The change in gelation kinetics with salt concentration was consistent with collagen [49], and was also concurrent with a significant change in gel stiffness. Increasing the salt concentration lead to a decrease in the storage modulus of the gels (figure 3). It has previously been shown that the stiffness of a gel or scaffold can impact cell fate [50], and thus being able to modify this material property may be advantageous.

When increasing pH from 7.4 to 8.5 there was no significant change in storage modulus. Collagen, on the other hand, has shown changes in mechanical properties when pH levels are altered, with increasing stiffness as the pH is increased [49]. However, Rosenblatt et al. had an inversion of this trend for their collagen gels formed at the 25°C compared to 20°C [20]. Williams et al. and Harris and Reiber noted changes and a decrease in fiber formation quality at high pH [19, 51], which was not observed for the myocardial matrix from pH 7.4 to 8.5. Li et al. explored collagen gels over a pH range of 6.6 to 8 with a trend of increasing fiber diameter as assessed with transmission electron microscopy [47]; however, the myocardial matrix did show a significant change in fiber diameter over the tested

NIH-PA Author Manuscript

NIH-PA Author Manuscript

NIH-PA Author Manuscript

parameters. Differences in the material, when compared to collagen, were expected because of the biochemical and structural importance of PG and GAG in the matrix formation [5, 8, 25, 52]. The presence of collagen along with other ECM components in the myocardial matrix material has been previously shown [53, 54].

When either pH or salt concentration was varied, the impact of altering material concentration in the gels was consistent. Increasing material concentration lead to a trend of increasing the storage modulus and a significant increase in complex viscosity, which is consistent with collagen [55]. Gobeaux et al. showed changes in collagen fiber diameter with increasing concentration over large changes at high concentrations from 50-1000 mg/ml [22]. For the myocardial matrix material no significant increase in fiber diameter was observed as material concentration increased.

It was shown for all samples in liquid form at 25°C that as shear rate increased, there was a decrease in complex viscosity. This phenomenon is known as shear-thinning, which also occurs with collagen when in the liquid form [31, 42]. Complex viscosity of the material at 25°C changed only with material concentration, and not with salt concentration or pH. Viscosity is defined as the resistance of flow to a fluid and is affected by the degree of intramolecular and intermolecular interactions. The increase of complex viscosity at higher material concentration can be explained by an increase in intermolecular forces [42]. Although mechanical strength, gelation kinetics, and viscosity were altered it was shown that the swelling ratio by mass is maintained for all conditions. The mass of the material increased by a factor of over 55 times its original weight when transitioning from a dry powder into a hydrogel. The standard deviations for the swelling ratios had a range of 2-20% of the mean value. Thus, the variation between the groups might have been masked by the large discrepancies within any given group.

The myocardial matrix derived ECM gel was consistent with several material property trends seen with collagen hydrogels. Both materials in liquid form are shear thinning and once over a temperature threshold form into a heterogeneous nanofibrous mesh. The trend of increasing gel stiffness and gelation kinetics when decreasing salt content was conserved. Also, increasing material concentration leads to an increase in viscosity and consequently gel stiffness for the myocardial matrix and collagen. The myocardial ECM is known to be predominately collagen, and given the similarities in material properties between the myocardial matrix and collagen gels, the main driving force for the self-assembling aspect of the myocardial material is likely its inherent collagen components. However, differences in the material when compared to collagen were observed in that the material did not show a significant increase in storage modulus when pH was increased to 8.5 and average fiber diameter did not alter for any of the conditions explored. Also, even though the same trends were conserved for gelation kinetics, the temperature of gelation and the actual times and rates of gelation varied. Variation from collagen gels was expected since the myocardial matrix hydrogel has previously been shown to contain other ECM components including sulfated GAGs [29, 54].

## 5. Conclusion

Tailoring material properties, as commonly explored for collagen hydrogels, by varying gelation parameters had not been previously investigated for decellularized ECM based hydrogels. From this study we were able to modulate the material properties of the naturally derived ECM material developed from porcine myocardial tissue. Gelation can be inhibited by maintaining the material at or below 22°C, but once brought to body temperature of 37°C, gelation is initiated. Once at 37°C the rate of gelation can be controlled and increased from ~20 minutes to over 8 hours by increasing salt concentration. This increase in salt

NIH-PA Author Manuscript

NIH-PA Author Manuscript

NIH-PA Author Manuscript

concentration, or decrease in rate of gelation, correlates to a decrease in the storage modulus of the material. Once gelled at 37°C at any of the explored conditions, a complex network of nanoscale fibers is formed with a mean fiber diameter in the range of 100 nm. By increasing material concentration there is an increase in the complex viscosity of the liquid suspension and the storage modulus once gelled. These parameters could therefore be modulated to tailor the myocardial ECM hydrogels for both *in vitro* and *in vivo* applications.

## Acknowledgments

The authors would like to acknowledge Jessica A. DeQuach and Sonya Seif-Naraghi for their technical help, along with the assistance of Carolina Rodgers, in harvesting porcine tissue samples. Also, Ryan Anderson and Patrick Charles of the Nano3 facility for their help with material preparation and scanning electron microscopy. Funding was provided by the National Institutes of Health (NIH) Director's New Innovator Award Program (K.L.C., DP20D004309), which is part of the NIH Roadmap for Medical Research. T.D.J. would like to thank the Powell Foundation for the Powell Fellowship through the Jacobs School of Engineering.

## References

1. Leor J, Amsalem Y, Cohen S. Cells, scaffolds, and molecules for myocardial tissue engineering. Pharmacol Ther. 2005; 105:151–63. [PubMed: 15670624]
2. Badylak SF. The extracellular matrix as a biologic scaffold material. Biomaterials. 2007; 28:3587–93. [PubMed: 17524477]
3. Lutolf MP, Hubbell JA. Synthetic biomaterials as instructive extracellular microenvironments for morphogenesis in tissue engineering. Nat Biotechnol. 2005; 23:47–55. [PubMed: 15637621]
4. Brown L. Cardiac extracellular matrix: a dynamic entity. Am J Physiol Heart Circ Physiol. 2005; 289:H973–4. [PubMed: 16100252]
5. Alberts B, Johnson A, Lewis J, Raff M, Roberts K, Walter P. Molecular biology of the cell (Fifth edition). 2008 Garland Science.
6. Flemming RG, Murphy CJ, Abrams GA, Goodman SL, Nealey PF. Effects of synthetic micro- and nano-structured surfaces on cell behavior. Biomaterials. 1999; 20:573–88. [PubMed: 10213360]
7. Barnes CP, Sell SA, Boland ED, Simpson DG, Bowlin GL. Nanofiber technology: designing the next generation of tissue engineering scaffolds. Advanced Drug Delivery Reviews. 2007; 59:1413–33. [PubMed: 17916396]
8. Silver FH, Freeman JW, Seehra GP. Collagen self-assembly and the development of tendon mechanical properties. Journal of Biomechanics. 2003; 36:1529–53. [PubMed: 14499302]
9. Ingber D. How cells (might) sense microgravity. The FASEB journal : official publication of the Federation of American Societies for Experimental Biology. 1999:S3–15. [PubMed: 10352140]
10. Koochekpour S, Merzak A, Pilkington GJ. Extracellular matrix proteins inhibit proliferation, upregulate migration and induce morphological changes in human glioma cell lines. Eur J Cancer. 1995; 31A:375–80. [PubMed: 7540403]
11. Parenteau-Bareil R, Gauvin R, Berthod F. Collagen-Based Biomaterials for Tissue Engineering Applications. Materials. 2010; 3:1863–87.
12. Li W-J, Ko FK. Electrospun nanofibrous structure: A novel scaffold for tissue engineering. 2001:1–9.
13. Wang H, Zhou J, Liu Z, Wang C. Injectable cardiac tissue engineering for the treatment of myocardial infarction. Journal of Cellular and Molecular Medicine. 2010
14. Drury JL, Mooney DJ. Hydrogels for tissue engineering: scaffold design variables and applications. Biomaterials. 2003; 24:4337–51. [PubMed: 12922147]
15. Singelyn JM, Christman KL. Injectable Materials for the Treatment of Myocardial Infarction and Heart Failure: The Promise of Decellularized Matrices. Journal of Cardiovascular Translational Research. 2010; 3:478–86. [PubMed: 20632221]
16. Leor J, Amsalem Y, Cohen S. Cells, scaffolds, and molecules for myocardial tissue engineering. Pharmacol Ther. 2005; 105:151–63. [PubMed: 15670624]

NIH-PA Author Manuscript

NIH-PA Author Manuscript

NIH-PA Author Manuscript

17. Ott HC, Matthiesen TS, Goh S-K, Black LD, Kren SM, Netoff TI, Taylor DA. Perfusion-decellularized matrix: using nature's platform to engineer a bioartificial heart. Nature medicine. 2008; 14:213–21.

18. Lee CH, Singla A, Lee Y. Biomedical applications of collagen. Int J Pharm. 2001; 221:1–22. [PubMed: 11397563]

19. Williams BR, Gelman RA, Poppke DC, Piez KA. Collagen fibril formation. Optimal in vitro conditions and preliminary kinetic results. The Journal of biological chemistry. 1978; 253:6578–85. [PubMed: 28330]

20. Rosenblatt J, Devereux B, Wallace DG. Injectable collagen as a pH-sensitive hydrogel. Biomaterials. 1994; 15:985–95. [PubMed: 7841296]

21. Hayashi T, Nagai Y. Factors affecting the interactions of collagen molecules as observed by in vitro fibril formation. III. Non-helical regions of the collagen molecules. Journal of biochemistry. 1974; 76:177–86. [PubMed: 4612027]

22. Gobeaux F, Mosser G, Anglo A, Panine P, Davidson P, Giraud-Guille M-M, Belamie E. Fibrillogenesis in dense collagen solutions: a physicochemical study. Journal of molecular biology. 2008; 376:1509–22. [PubMed: 18234220]

23. Raub CB, Unruh J, Suresh V, Krasieva T, Lindmo T, Gratton E, Tromberg BJ, George SC. Image correlation spectroscopy of multiphoton images correlates with collagen mechanical properties. Biophysical journal. 2008; 94:2361–73. [PubMed: 18065452]

24. Roeder BA, Kokini K, Sturgis JE, Robinson JP, Voytik-Harbin SL. Tensile Mechanical Properties of Three-Dimensional Type I Collagen Extracellular Matrices With Varied Microstructure. Journal of Biomechanical Engineering. 2002; 124:214. [PubMed: 12002131]

25. Daamen WF, van Moerkerk HTB, Hafmans T, Buttafoco L, Poot AA, Veerkamp JH, van Kuppevelt TH. Preparation and evaluation of molecularly-defined collagen-elastinglycosaminoglycan scaffolds for tissue engineering. Biomaterials. 2003; 24:4001–9. [PubMed: 12834595]

26. Ellis DL, Yannas IV. Recent advances in tissue synthesis in vivo by use of collagen-glycosaminoglycan copolymers. Biomaterials. 1996; 17:291–9. [PubMed: 8745326]

27. Voytik-Harbin SL, Brightman AO, Waisner BZ, Robinson JP, Lamar CH. Small Intestinal Submucosa: A Tissue-Derived Extracellular Matrix That Promotes Tissue-Specific Growth and Differentiation of Cells in Vitro. Tissue engineering. 1998; 4:157–74.

28. Badylak SF, Freytes DO, Gilbert TW. Extracellular matrix as a biological scaffold material: Structure and function. Acta Biomaterialia. 2009; 5:1–13. [PubMed: 18938117]

29. Singelyn JM, DeQuach JA, Seif-Naraghi SB, Littlefield RB, Schup-Magoffin PJ, Christman KL. Naturally derived myocardial matrix as an injectable scaffold for cardiac tissue engineering. Biomaterials. 2009; 30:5409–16. [PubMed: 19608268]

30. Seif-Naraghi SB, Salvatore MA, Schup-Magoffin PJ, Hu DP, Christman KL. Design and characterization of an injectable pericardial matrix gel: a potentially autologous scaffold for cardiac tissue engineering. Tissue engineering. Part A. 2010; 16:2017–27. [PubMed: 20100033]

31. Freytes D, Martin J, Velankar S, Lee A. Preparation and rheological characterization of a gel form of the porcine urinary bladder matrix. Biomaterials. 2008

32. Young DA, Ibrahim DO, Hu D, Christman KL. Injectable hydrogel scaffold from decellularized human lipoaspirate. Acta Biomaterialia. 2011; 7:1040–9. [PubMed: 20932943]

33. Knapp PM, Lingeman JE, Siegel YI, Badylak SF, Demeter RJ. Biocompatibility of Small-Intestinal Submucosa in Urinary-Tract as Augmentation Cystoplasty Graft and Injectable Suspension. J Endourol. 1994; 8:125–30. [PubMed: 8061669]

34. Singelyn JM, Christman KL. Modulation of material properties of a decellularized myocardial matrix scaffold. Macromol Biosci. 2011; 11:731–8. [PubMed: 21322109]

35. Li Z, Guan J. Hydrogels for cardiac tissue engineering. Polymers. 2011; 3:740–61.

36. Christman KL, Lee RJ. Biomaterials for the treatment of myocardial infarction. J Am Coll Cardiol. 2006; 48:907–13. [PubMed: 16949479]

37. Singelyn JM, Christman KL. Injectable materials for the treatment of myocardial infarction and heart failure: the promise of decellularized matrices. J Cardiovasc Transl Res. 2010; 3:478–86. [PubMed: 20632221]

NIH-PA Author Manuscript

NIH-PA Author Manuscript

NIH-PA Author Manuscript


38. Nelson DM, Ma Z, Fujimoto KL, Hashizume R, Wagner WR. Intra-myocardial biomaterial injection therapy in the treatment of heart failure: Materials, outcomes and challenges. Acta Biomater. 2011; 7:1–15. [PubMed: 20619368]
39. Pogorelov AG, Selezneva II. Evaluation of collagen gel microstructure by scanning electron microscopy. Bulletin of experimental biology and medicine. 2010; 150:153–6. [PubMed: 21161075]
40. Baker SC, Atkin N, Gunning PA, Granville N, Wilson K, Wilson D, Southgate J. Characterisation of electrospun polystyrene scaffolds for three-dimensional in vitro biological studies. Biomaterials. 2006; 27:3136–46. [PubMed: 16473404]
41. Lutolf MP, Hubbell JA. Synthesis and physicochemical characterization of end-linked poly(ethylene glycol)-co-peptide hydrogels formed by Michael-type addition. Biomacromolecules. 2003; 4:713–22. [PubMed: 12741789]
42. Chan RW, Titze IR. Viscosities of implantable biomaterials in vocal fold augmentation surgery. The Laryngoscope. 1998; 108:725–31. [PubMed: 9591554]
43. Gelman RA, Williams BR, Piez KA. Collagen fibril formation. Evidence for a multistep process. The Journal of biological chemistry. 1979; 254:180–6. [PubMed: 758319]
44. Mauck RL, Baker BM, Nerurkar NL, Burdick JA, Li W-J, Tuan RS, Elliott DM. Engineering on the straight and narrow: the mechanics of nanofibrous assemblies for fiber-reinforced tissue regeneration. Tissue engineering. Part B, Reviews. 2009; 15:171–93. [PubMed: 19207040]
45. Latinovic O, Hough LA, Ou-Yang HD. Structural and micromechanical characterization of type I collagen gels. Journal of Biomechanics. 2010; 43:500–5. [PubMed: 19880123]
46. Yeo I-S, Oh J-E, Jeong L, Lee TS, Lee SJ, Park WH, Min B-M. Collagen-Based Biomimetic Nanofibrous Scaffolds: Preparation and Characterization of Collagen/Silk Fibroin Bicomponent Nanofibrous Structures. Biomacromolecules. 2008; 9:1106–16. [PubMed: 18327908]
47. Li Y, Asadi A, Monroe M. pH effects on collagen fibrillogenesis in vitro: Electrostatic interactions and phosphate binding. Materials Science and ... 2009
48. Wood GC, Keech MK. The formation of fibrils from collagen solutions 1. The effect of experimental conditions: kinetic and electron-microscope studies. Biochemical Journal. 1960; 75:588. [PubMed: 13845809]
49. Achilli M, Mantovani D. Tailoring Mechanical Properties of Collagen-Based Scaffolds for Vascular Tissue Engineering: The Effects of pH, Temperature and Ionic Strength on Gelation. Polymers. 2010; 2:664–80.
50. Engler AJ, Griffin MA, Sen S, Bönnemann CG, Sweeney HL, Discher DE. Myotubes differentiate optimally on substrates with tissue-like stiffness: pathological implications for soft or stiff microenvironments. The Journal of cell biology. 2004; 166:877–87. [PubMed: 15364962]
51. Harris JR, Reiber A. Influence of saline and pH on collagen type I fibrillogenesis in vitro: fibril polymorphism and colloidal gold labelling. Micron (Oxford, England : 1993). 2007; 38:513–21.
52. Brightman A, Rajwa B, Sturgis J. Time-lapse confocal reflection microscopy of collagen fibrillogenesis and extracellular matrix assembly in vitro. Biopolymers. 2000
53. Singelyn JM, DeQuach JA, Seif-Naraghi SB, Littlefield RB, Schup-Magoffin PJ, Christman KL. Naturally derived myocardial matrix as an injectable scaffold for cardiac tissue engineering. Biomaterials. 2009; 30:5409–16. [PubMed: 19608268]
54. DeQuach JA, Mezzano V, Miglani A, Lange S, Keller GM, Sheikh F, Christman KL. Simple and high yielding method for preparing tissue specific extracellular matrix coatings for cell culture. PLoS One. 2010; 5:e13039. [PubMed: 20885963]
55. Yang, Y-l; Kaufman, LJ. Rheology and confocal reflectance microscopy as probes of mechanical properties and structure during collagen and collagen/hyaluronan self-assembly. Biophysical journal. 2009; 96:1566–85. [PubMed: 19217873]

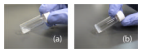

**Figure 1.**
Gelation of myocardial matrix hydrogel. (a) At 4°C and 22°C the material is maintained in the liquid form. (b) When at 37°C the material forms a gel that maintains shape.

NIH-PA Author Manuscript
NIH-PA Author Manuscript
NIH-PA Author Manuscript

NIH-PA Author Manuscript
NIH-PA Author Manuscript
NIH-PA Author Manuscript



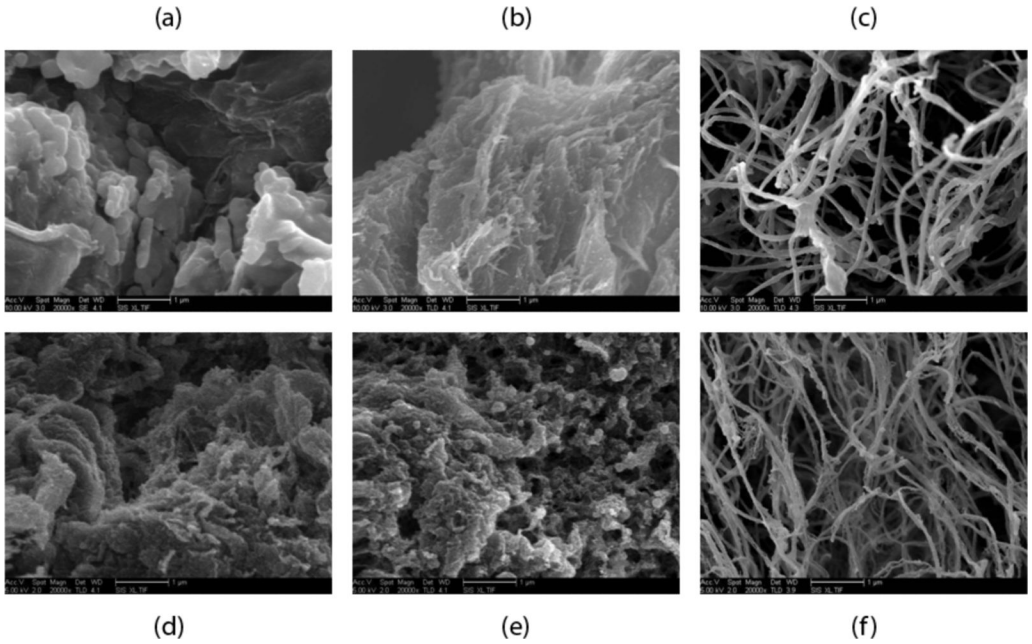


**Figure 2.**
Scanning electron microscopy images of the material 24 hours after attempted gelation at different temperatures. (a) and (d) 4°C. (b) and (e) room temperature. (c) and (f) 37°C. (a)-(c) are 6 mg/ml and (d)-(f) are 8 mg/ml material concentration. Scale bars are 1 μm.

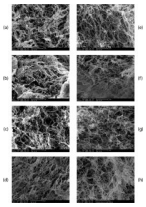

**Figure 3.**
SEM images of the gels after 24 hours of incubation at 37°C. Left column is at 6 mg/ml and right column is at 8 mg/ml. (a) and (e) 0.5× PBS. (b) and (f) 1.5× PBS. (c) and (g) standard physiological conditions of 7.4 pH and 1.0x PBS. (d) and (h) pH 8.5. Scale bars are 5 μm.

NIH-PA Author Manuscript
NIH-PA Author Manuscript
NIH-PA Author Manuscript

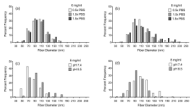

**Figure 4.**
Histograms of the fiber diameter distributions measured from SEM images after gelation for 24 hours at 37°C. (a) and (c) 6 mg/ml. (b) and (d) 8 mg/ml. (a) and (b) salt concentration is varied. (c) and (d) pH is varied.

NIH-PA Author Manuscript
NIH-PA Author Manuscript
NIH-PA Author Manuscript

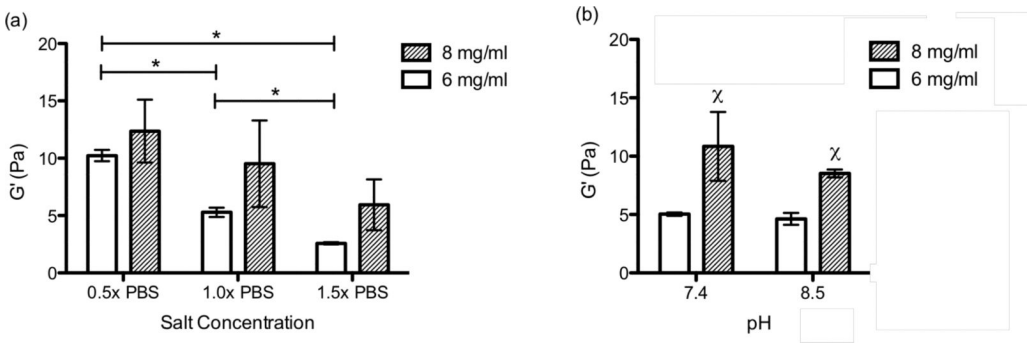


**Figure 5.**

Storage modulus (G') in pascals of the static gels after 24 hours gelation at 37°C. (a) pH 7.4 with salt concentrations of 0.5×, 1.0x, and 1.5× PBS. *$p<0.05$ (b) 1.0× PBS with pH of 7.4 and 8.5. One-way ANOVA for pH at 6 mg/ml ($p=0.0012$). Inner group significance for pH or salt concentration $\chi = p<0.05$ compared to lower concentration.



NIH-PA Author Manuscript
NIH-PA Author Manuscript
NIH-PA Author Manuscript

NIH-PA Author Manuscript
NIH-PA Author Manuscript
NIH-PA Author Manuscript



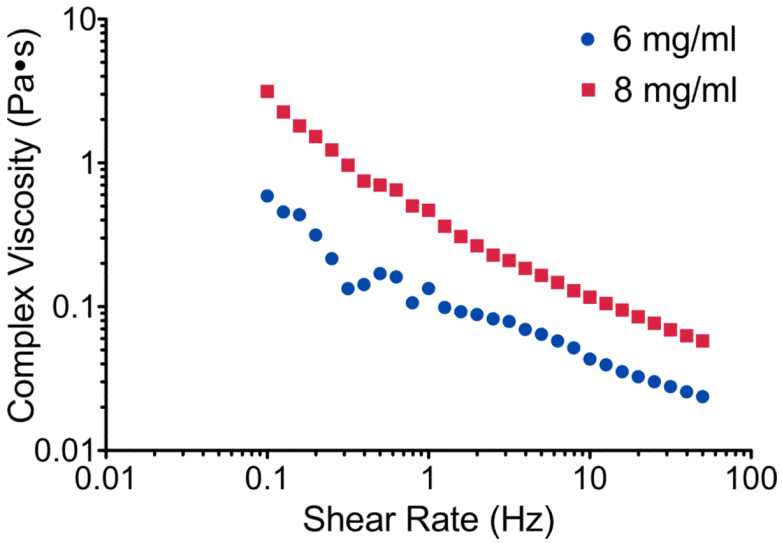


**Figure 6.**
Complex viscosity of the myocardial matrix in liquid form in standard conditions at 25°C plotted over shear rate on a log-log scale.

NIH-PA Author Manuscript
NIH-PA Author Manuscript
NIH-PA Author Manuscript



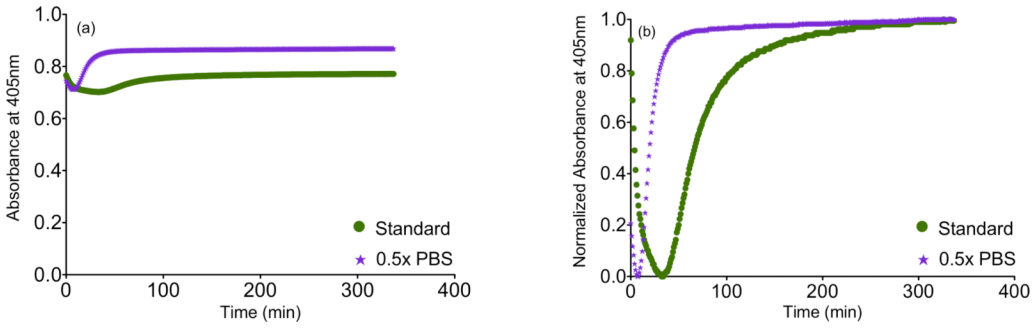


**Figure 7.**

Turbidity results averaged per condition plotted over time for the gelation of the myocardial matrix at 37°C for 6 mg/ml. (a) Absorbance at 405nm. (b) Normalized absorbance at 405nm.

NIH-PA Author Manuscript

NIH-PA Author Manuscript

NIH-PA Author Manuscript

**Table 1**

Average Fiber diameter of gels incubated at 37°C for 24 hours (nm).

| Condition | 6 mg/ml | 8 mg/ml |
|---|---|---|
| Standard | 92.92 ± 24.38 | 112.20 ± 28.74 |
| 0.5× PBS | 102.49 ± 22.79 | 111.37 ± 30.77 |
| 1.5× PBS | 101.46 ± 24.32 | 119.80 ± 36.99 |
| 8.5 pH | 96.04 ± 26.24 | 92.60 ± 21.86 |

NIH-PA Author Manuscript

NIH-PA Author Manuscript

NIH-PA Author Manuscript

**Table 2**

Storage modulus (G') and loss modulus (G") of static gels after 24 hours gelation at 37°C.

| Condition | *G' (Pa)* | *G" (Pa)* |
|---|---|---|
| **6mg/ml** | | |
| Standard | 5.28 ± 0.41 | 0.893 ± 0.085 |
| 0.5× PBS | 10.23 ± 0.49 | 1.652 ± 0.092 |
| 1.5× PBS | 2.58 ± 0.09 | 0.467 ± 0.21 |
| pH 8.5 | 4.63 ± 0.51 | 0.785 ± 0.12 |
| **8mg/ml** | | |
| Standard | 9.52 ± 3.77 | 1.75 ± 0.72 |
| 0.5× PBS | 12.36 ± 2.74 | 2.50 ± 0.78 |
| 1.5× PBS | 5.94 ± 2.21 | 1.70 ± 0.38 |
| pH 8.5 | 8.53 ± 0.34 | 2.72 ± 1.0 |

NIH-PA Author Manuscript

NIH-PA Author Manuscript

NIH-PA Author Manuscript

## Table 3

Complex viscosity of the myocardial matrix material at 25°C for frequencies from 0.1-50 Hz.

| Condition | *k* | *n* | $r^2$ |
|---|---|---|---|
| **6mg/ml** | | | |
| Standard | 0.1300 | -0.466 | 0.955 |
| 0.5× PBS | 0.1548 | -0.523 | 0.959 |
| 1.5× PBS | 0.1580 | -0.519 | 0.963 |
| pH 8.5 | 0.2030 | -0.550 | 0.978 |
| **8mg/ml** | | | |
| Standard | 0.4976 | -0.617 | 0.982 |
| 0.5× PBS | 0.4402 | -0.656 | 0.994 |
| 1.5× PBS | 0.4641 | -0.580 | 0.983 |
| pH 8.5 | 0.4568 | -0.606 | 0.988 |

NIH-PA Author Manuscript

NIH-PA Author Manuscript

NIH-PA Author Manuscript

**Table 4**

Swelling ratio by mass after gelation at 37°C.

| Condition | 6 mg/ml | 8 mg/ml |
|---|---|---|
| Standard | 58.4 ± 10.20 | 57.4 ± 2.39 |
| 0.5× PBS | 55.9 ± 8.36 | 57.0 ± 1.19 |
| 1.5× PBS | 56.4 ± 5.48 | 55.8 ± 4.68 |
| pH 8.5 | 55.7 ± 4.34 | 56.2 ± 2.63 |

NIH-PA Author Manuscript

NIH-PA Author Manuscript

NIH-PA Author Manuscript

## Table 5

Turbidity results for lag time ($t_{lag}$) slope of linear region (S), and half gelation time ($t_{1/2}$) at 6 mg/ml.

| Condition | $t_{lag}$ | S | $t_{1/2}$ |
|---|---|---|---|
| Standard | 40.28 ± 1.91 | 0.01867 ± 0.0012 | 67.14 ± 3.40 |
| 0.5× PBS | 11.40 ± 2.17* | 0.05067 ± 0.0021* | 21.27 ± 2.33* |

*p<0.0001 compared to standard condition.